A Method to Derive Smoke Emission Rates From MODIS Fire Radiative Energy Measurements

Charles Ichoku and Yoram J. Kaufman

***Abstract*—Present methods of emissions estimation from satellite data often use fire pixel counts, even though fire strengths and smoke emission rates can differ by some orders of magnitude between pixels. Moderate Resolution Imaging Spectroradiometer (MODIS) measurements of fire radiative energy (FRE) release rates $R_{\rm fre}$ range from less than 10 to more than 1700 MW per pixel at 1-km resolution. To account for the effect of such a wide range of fire strengths/sizes on smoke emission rates, we have developed direct linear relationships between the MODIS-measured $R_{\rm fre}$ and smoke aerosol emission rates $R_{\rm sa}$ (in kilograms per second), derived by analyzing MODIS measurements of aerosol spatial distribution around the fires with National Center for Environmental Prediction/National Center for Atmospheric Research wind fields. We applied the technique to several regions around the world and derived a FRE-based smoke emission coefficient, C_e (in kilograms per megajoule), which can be simply multiplied by $R_{\rm fre}$ to calculate $R_{\rm sa}$. This new coefficient C_e is an excellent remote sensing parameter expressing the emission strength of different ecosystems and regions. Analysis of all 2002 MODIS data from Terra and Aqua satellites yielded C_e values of 0.02–0.06 kg/MJ for boreal regions, 0.04–0.08 kg/MJ for both tropical forests and savanna regions, and 0.08–0.1 kg/MJ for Western Russian regions. These results are probably overestimated by about 50% because of uncertainties in some of the data, parameters, and assumptions involved in the computations. This 50% overestimation is comparable to uncertainties in traditional emission factors. However, our satellite method shows great promise for accuracy improvement, as better knowledge is gained about the sources of the uncertainties.**

***Index Terms*—Author, please supply your own keywords or send a blank e-mail to keywords@ieee.org to receive a list of suggested keywords..**

I. Introduction

WILDFIRES and prescribed biomass-burning devastate vast areas of forest lands, grass lands, and agricultural lands across the globe, consuming an estimated 5500–9200 Tg of biomass annually [1], [2]. For instance, in Canada alone, it was estimated that about 4.9 million hectares burned in 1995 [3]. By so doing, fires directly exert adverse (and, in some cases, favorable) influences on ecology, population, habitat, agriculture, transportation, and security. The 2001 report of the Intergovernmental Panel on Climate Change (IPCC) [4] states that "most climate scenarios indicate that the probability of large fires will increase" (IPCC, 2001, sec 13.2.2.1.2). The effects of fires on climate and the environment are not limited to the ravages of their flame but also include the impacts of the energy, aerosols (or particulate matter, PM), and trace gases emitted into the atmosphere. Fires release heat energy, which is propagated by conduction, convection, and radiation. Fire radiative energy (FRE), like other types of electromagnetic radiant energy, propagates in space and can be sensed from aircraft and satellites. The Moderate-Resolution Imaging Spectroradiometer (MODIS) sensor, launched aboard the Earth Observing System (EOS) Terra and Aqua satellites on December 18, 1999 and May 4, 2002, respectively, is the first to operationally measure from space the FRE rate of release ($R_{\rm fre}$), using its 3.96-μm channels, which do not saturate for most fires.

Commensurate with the large volumes of biomass consumed by fires, tremendous amounts of smoke are emitted into the atmosphere annually. Globally, an estimated 3.1×10^9 t of biomass carbon is exposed to burning annually, of which 1.1×10^9 t is emitted to the atmosphere through combustion [5]. Smoke comprises aerosol particles and trace gases (including CO_2, CO, CH_4, and other species), which constitute air pollutants and contribute to the perturbation of the global radiative balance through the scattering and absorption of solar radiation. Andreae and Merlet [6] provide a detailed list of the various particulate and gaseous species emitted by fires. Although some trace gases (CO_2 and CH_4) have long been associated with climate change, atmospheric aerosols and, particularly, smoke aerosol (because of its considerable black carbon content) probably have a much greater impact, not only on climate, but also on weather, health, aviation, visibility, and environmental pollution. However, the global effects of fires and emitted smoke aerosols and trace gases are still poorly understood. To fully understand the effects of biomass burning on humans and the environment, it is important to acquire an accurate quantitative inventory of the fire locations and frequency, the amount of biomass they consume, and the energy, aerosols, and trace gases they release into the atmosphere.

Accurate assessment of the environmental and climate effects of smoke can only be achieved if the amount or the rate of emission of smoke is estimated accurately. It is a common saying that: "there is no smoke without fire." Ironically, some of the initial attempts at estimating emissions did not include any quantitative measure of the fire, but were based on limited localized smoke measurements, which were then extrapolated to cover larger areas using different socio-ecologic statistical estimates and other qualitative information and assumptions, in-

Manuscript received November 18, 2004; revised July 21, 2005. This work was supported in part by the Nationa Aeronautics and Space Administration Applications Directorate (Code YO) under Project 613-23-20: Air Quality Application—Fire Emissions.

C. Ichoku is with Science Systems and Applications Inc., Lanham, VA 20706 USA and also with the NASA Goddard Space Flight Center, Greenbelt, MD 20771 USA (e-mail: ichoku@climate.nasa.gov).

Y. J. Kaufman is with the Laboratory for Atmospheres, NASA Goddard Space Flight Center, Greenbelt, MD 20771 USA.

Digital Object Identifier 10.1109/TGRS.2005.857328

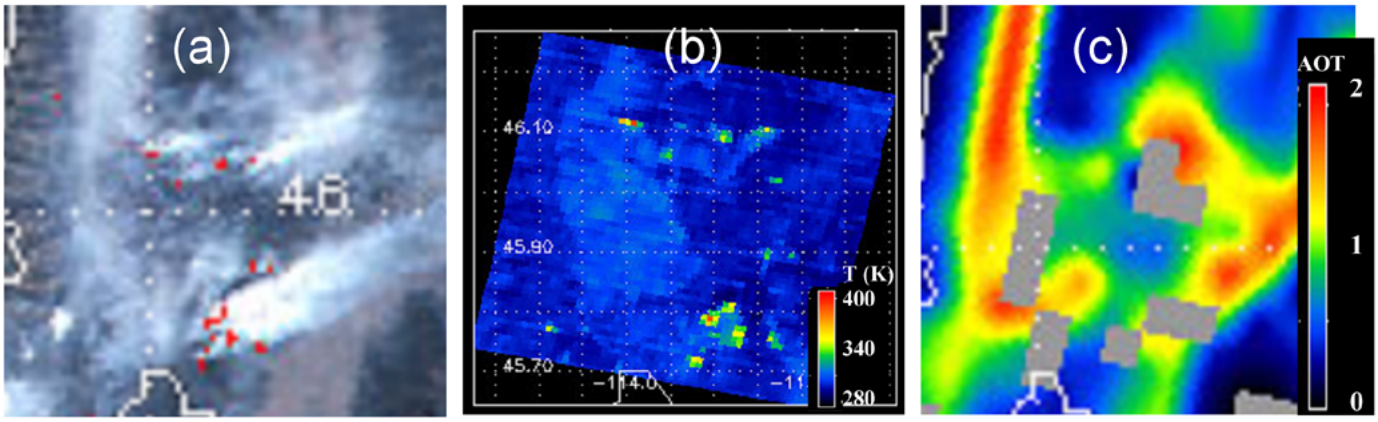

Fig. 1. Subsets of MODIS data acquired on August 23, 2000 at 18:45 UTC over a fire event in southwest Montana (near the border with Idaho), showing (a) true-color RGB image dominated by whitish smoke, with red dots identifying fire pixels, (b) brightness temperatures from the MODIS 4-μm channel (band 21), in which the fire pixels, depicting different levels of release of fire radiative energy, span a wide range of temperatures with respect to the background, and (c) the smoke aerosol optical thickness (AOT) at the 550-nm wavelength, with gray areas representing pixels whose AOT were not retrieved because the algorithm mistook the thick smoke to be clouds.

cluding vegetation types and conditions, population densities, distribution, and dynamics, as well as the associated agricultural and other domestic burning practices [7]–[10]. More recently, rapid developments in satellite technology and remote sensing from space have enabled global observation and monitoring of vegetation, fires, and emissions from a variety of sensors [11]–[16]. Even so, fires and smoke retrieved by remote sensing were generally treated as independent entities, and until very lately (up until 2000), it was rare to find studies (such as [11]) which attempted to address the direct relationship between fires and smoke as observed from satellites. As will be elaborated in Section II, a number of recent studies published so far during this new millennium have taken bold steps to derive emissions from remotely sensed fire products such as fire pixel counts and burned areas, although none actually made the direct connection between satellite-observed fires and smoke.

Fig. 1 shows subsets of MODIS data acquired on August 23, 2000 at 18:45 UTC over a fire event in southwest Montana (near the border with Idaho), representing: 1) fire locations and smoke; 2) pixel brightness temperatures depicting a range of fire intensities relative to the background; and 3) the smoke aerosol optical thickness (AOT) at the 550-nm wavelength. This paper seeks to utilize the advantages offered by simultaneous satellite observation of fires and smoke, particularly the operational MODIS measurement of FRE rate of release $(R_{\rm fre})$ and aerosols over land, to formulate a procedure for deriving smoke emission rates from $R_{\rm fre}$, based on their direct relationship. The paper focuses specifically on the estimation of rates of emission of smoke aerosols (or PM), although the methodology developed in this work is equally applicable to trace gas species measurable from satellite, such as carbon monoxide (CO).

II. Background and Motivation

There have been substantial scientific efforts at estimating smoke emissions, mostly by the use of models. Prior to the satellite era, the source of the input data used in smoke emission models come by way of estimates of the amount of biomass consumed, usually derived by multiplying the acreage of area burned with the estimated biomass density. The amount of the emitted aerosol or trace gas species of interest is derived by multiplying the mass of biomass burned by the species' emission factor (in grams of species per kilogram of dry matter burned). The basic equation is of the form [6]

$$M_x = \mathrm{EF}_x * M_{\rm biomass} \tag{1}$$

where M_x is the mass of emitted species x, EF_x is the emission factor for the emitted species x, while $M_{\rm biomass}$ is the mass of the dry biomass burned.

With the great opportunity offered by remote sensing in this satellite era, it has become necessary to develop methodologies for deriving fire emissions from spaceborne sensor measurements. However, even if the emission factors (EF_x) for different species are known accurately, it is currently not obvious to estimate $M_{\rm biomass}$ to acceptable accuracy from remotely sensed data, and certainly not in real time. The use of fire pixel counts from satellite sensors still requires estimates of $M_{\rm biomass}$ or its surrogate from such sources as biomass-burned inventories [17] compiled with traditional methods, making it applicable only long after the fire is over. A method of deriving estimates of smoke emission from satellite aerosol measurements and fire

TABLE I
Regions Selected for This Study and Their Longitude/Latitude Boundaries

Region	Lon_min	Lon_max	Lat_min	Lat_max
Alaska	-170	-140	50	75
Asia	70	130	-5	50
Australia	110	160	-40	-10
Braz_Cer	-50	-30	-20	0
Braz_For	-75	-50	-15	5
Canada	-140	-80	50	70
Congo	10	35	-10	5
Europe	-10	30	35	75
Mexico	-120	-85	15	30
Quebec	-80	-55	45	65
Russia	30	60	45	75
Siberia	60	150	60	85
SouthAfr	10	35	-35	-20
SouthAmer	-80	-45	-60	-20
USA	-125	-70	25	50
WestAfr	-20	15	0	20
Zambia	22	35	-18	-8

pixel counts was developed by Kaufman *et al.* [11], although one of the main limitations was the inability to distinguish large fires from small fires, which resulted in expressing the emissions in units of "mass per fire." However, fire pixel counts from the Geostationary Operational Environmental Satellites (GOES) [16] are being used to estimate smoke aerosol emissions in nearly real time, and to provide forecasting using a prognostic aerosol model [18].

An alternative approach for deriving emissions from satellite is based on burned area products, which are used to estimate M_{biomass} indirectly, with the following relationship [7]:

$$M_{\text{biomass}} = A \times B \times \alpha \times \beta \tag{2}$$

where A is the burned area, B is the biomass density, α is the fraction of above-ground biomass, and β is the burn efficiency. Indeed several papers using this approach to estimate aerosol and gas emissions were recently published in a special section of the *Journal of Geophysical Research* [19]–[22]. In the same journal issue, a number of papers described some existing burned-area algorithms and products from different sensors, such as the GLOBSCAR product from the Along Track Scanning Radiometer (ATSR-2) instrument onboard the European Space Agency (ESA) ERS-2 satellite and the Global Burnt Area product derived from SPOT/VEGETATION [23], [24]. MODIS has also shown great potential in providing burned-area products, with the development of a number of algorithms, which could be implemented operationally in the near future, at least on a regional basis [25], [26]. Burned area products from all three sensors were compared in southern Africa and showed substantial differences, which produced corresponding differences in emissions estimation [27]. Although burned-area products are a valuable satellite-derived parameter for estimating emissions, they represent only one factor in (2), which is in turn a subset of (1). The other three factors in (2) are not easy to determine. For instance, the burn efficiency, β, has been found to be influenced by fuel conditions, including moisture content [28]. Another weakness of the use of burned-area products is that they are often available only after the fire is over. Their true strength lies in their application for developing postburn emissions inventories.

This study seeks to achieve truly quantitative satellite-based emission estimates using a measure of fire activity and size, capable of being applied even when the fire is still actively burning, with less dependence on external parameters. Fortunately, it has now become possible to measure from satellite sensors, such as MODIS, the rate of release (R_{fre}) of fire radiative energy (FRE) [15], [29], [30]. Since the rate at which fire releases energy is indicative of its rate of consumption of biomass, which is a function of area being burned, biomass density, above-ground fraction, and combustion efficiency, R_{fre} therefore expresses all the factors on the right-hand side of (2). Indeed, it has been determined that there is a direct linear relationship between the time-integrated R_{fre} and M_{biomass} [31]. This was based on a series of field experiments conducted with senesced biomass in the U.K. and Botswana, in which R_{fre} was measured with a field spectroradiometer mounted on a tower viewing the fires below as they burn the biomass placed on a scale measuring the M_{biomass}. Results of experiments conducted in an in-door combustion chamber in the U.S. were also in agreement with those of the U.K. and Botswana (Wooster, personal communication, 2004). The linear relationship between the time integrated R_{fre} and M_{biomass} from those experiments enabled the determination of a "FRE-Combustion-Factor" (F_{fcb}) in kilograms per megajoule [31], which when multiplied with FRE in MJ gives the amount of biomass consumed M_{biomass} in kilograms.

Given, from (1), that M_x is related to M_{biomass}, which is in turn related to R_{fre}, it follows then that M_x is related to R_{fre}, which is measured from satellite. Therefore, satellite derivation of emissions (M_x) as a function of R_{fre} can be achieved. If M_{biomass} is replaced with R_{fre} in (1), then, the mass-based emission factor, EF_x, should be replaced with a FRE-based emission coefficient (which shall henceforth be designated by C_e). Thus, the mass of emitted species x can be derived with (3)

$$M_x = C_e * R_{\text{fre}} \tag{3}$$

where in this case M_x is the rate of emission of species x (expressed in kilograms per second), because R_{fre} is expressed in megawatts or megajoules per second, and C_e is expressed kilograms per megajoule. However, if a time-integrated total FRE (in MJ) is used instead of R_{fre}, then M_x would become the emitted total mass expressed in Kg.

In fact, C_e (in kilograms per megajoule) can be derived from EF_x (in kilograms per kilogram) simply by multiplying the latter by the "FRE-combustion factor" (F_{fcb} in kilograms per megajoule) as derived by [31]. However, the F_{fcb} value derived in [31] will not be used in this paper, as it is currently being revised because of calibration uncertainties found in the spectroradiometer upon whose measurements it was based (Wooster 2005, in preparation). This ability to relate the satellite measured quantity R_{fre} to physical quantities of mass of biomass and smoke particulates is the principal motivation to conduct the study described in this paper. Therefore, it is the objective in this paper to use MODIS-measured R_{fre} and smoke aerosols in deriving C_e, which is the key to estimating both fire consumed biomass mass (M_{biomass}) and the emitted smoke aerosol total particulate mass (M_{aerosol}) for different ecosystems.

The use of R_{fre} in emissions estimation offers a number of advantages compared to the use of fire pixel counts or burned area. Unlike fire pixel counts, which only show fire locations, R_{fre} is a measure of fire strength (size and intensity), which embodies the amount of M_{biomass} being consumed. Therefore, the use of R_{fre} almost eliminates dependence on other methods of estimating area burned (A), biomass density (B), above-ground biomass proportion (α), and combustion efficiency (β) in (2). Furthermore, R_{fre} can be used to derive emission rates in the near real-time, unlike burned area methods, which depend on several factors that can only be determined when the fire is over, though they find better application in postburn emission inventories.

III. MODIS Data Preparation

MODIS detects fires at a spatial resolution of 1 km at nadir [15], [30], [32]. For every fire pixel detected, it also derives the corresponding fire radiative power (or the rate of release of fire radiative energy), $R_{\rm fre}$ in megawatts or megajoules per second. The formulation for derivation of $R_{\rm fre}$ was developed in [15] and is given in (4)

$$R_{\rm fre} = 4.34 \times 10^{-19} \left(T_4^8 - T_{4b}^8\right) \tag{4}$$

where $R_{\rm fre}$ (in megawatts) is the pixel fire radiative power, T_4 (in Kelvin) is the fire pixel brightness temperature at the 4-μm channel (more precisely 3.96 μm), and T_{4b} is the 4-μm brightness temperature of the background surrounding the fire pixel.

Apart from fires, MODIS also measures atmospheric aerosols (including smoke) and derives aerosol products at 10-km spatial resolution at nadir. The most important aerosol parameter provided by MODIS at several wavelengths (λ) is aerosol optical thickness (AOT or $\tau_{a\lambda}$) at 470-, 550-, and 660-nm wavelengths over land, as well as at 470-, 550-, 660-, 870-, 1200-, 1600-, and 2100-nm wavelengths over ocean [33]. However, since fires usually occur over land, this study will be based on the use of AOT over land, specifically at the 550-nm (green) wavelength, which is the most commonly used wavelength in aerosol radiation studies.

The first step in the joint analysis of fire and smoke from MODIS was the collocation of fire and aerosol pixels. All fire pixels (1-km resolution at nadir) falling into each aerosol pixel (10-km resolution at nadir) were identified and counted. The sum of the $R_{\rm fre}$ of all fire pixels so identified is the total $R_{\rm fre}$ generated in that aerosol pixel. This is done regardless of whether or not there is aerosol retrieval in that aerosol pixel. Then, using the coordinates of the aerosol pixel, the wind vectors corresponding to it are extracted from the National Center for Environmental Prediction/National Center for Atmospheric Research (NCEP/NCAR) reanalysis dataset [34]. The aerosol and wind data are subjected to integrated spatial analysis to derive the smoke aerosol emission rates as described in the following section.

IV. Methodology for Derivation of Smoke Emission Rates

In the computations for smoke aerosol emissions derivation described in the following subsections, each aerosol pixel is the basic reference unit area to which the fire/aerosol/wind parameters are associated. It is pertinent to mention that, as imposed by the geometric constraints related to most satellite data acquisitions, MODIS ground pixel size increases with scan angle, both along scan and along track [35]. Therefore, although the aerosol pixel measures approximately 10×10 km at nadir, the actual off-nadir pixel sizes on the ground are much larger. The rate of increase of the ground cell size with scan angle (θ) is faster along scan than along track. For the calculations performed herein, it is important to know the correct area ($A^{\rm ap}$) of each aerosol pixel. Assuming a given pixel has along-scan size ΔS and along-track size ΔT, then its correct area $A^{\rm ap}$ is the product of ΔS and ΔT.

MODIS along-scan (ΔS) and along-track (ΔT) ground pixel sizes can be derived as functions of θ from the following relationships (Masahiro Nishihama, personal communication, 2004):

$$\Delta S = R_e s \left(\frac{\cos\theta}{((R_e/r)^2 - \sin^2\theta)^{1/2}} - 1 \right) \tag{4}$$

$$\Delta T = rs \left(\cos\theta - ((R_e/r)^2 - \sin^2\theta)^{1/2} \right) \tag{5}$$

where $R_e = 6378.137$ km (radius of the earth), $h = 705$ km (altitude of satellite), $r = R_e + h, s = p/h, p$ is pixel nadir resolution in kilometers (which is 10 km for MODIS aerosol pixels), and θ is the scan angle calculated at any given pixel i as (Masahiro Nishihama, personal communication, 2004)

$$\theta_i = -\frac{1}{2}Ns + \frac{1}{2}s + (i-1)s \tag{6}$$

where N is the number of pixels in each row of the image swath, i is the column number of the specific column for which θ is being calculated, while the rest of the variables are as defined for (4) and (5).

A. Stage One: Pixel-Based Calculations

A number of calculations are performed at the level of individual 10-km resolution aerosol pixels before the calculations involving whole fires or regions.

1) Smoke Mass Density: For each aerosol pixel containing fire, its aerosol optical thickness (AOT) at the 550-nm wavelength τ_{a550} and those of all of its eight neighboring pixels are extracted. The minimum AOT value of those eight neighboring pixels is assumed to be the relative "background" AOT (τ_{a550}^b) with respect to the emissions from the central pixel. The maximum value among the central pixel τ_{a550} and those of the eight neighbors is regarded as the total AOT (τ_{a550}^t) of background plus the emitted smoke. The reason the central pixel AOT is not simply taken as the τ_{a550}^t is to capture cases where only a single fire pixel at one side or corner of the aerosol pixel could be emptying all its smoke into one of the neighboring aerosol pixels. The AOT of the smoke emitted by the fire (τ_{a550}^f) in each aerosol pixel is assumed to be

$$\tau_{a550}^f = \tau_{a550}^t - \tau_{a550}^b. \tag{7}$$

This fire-emitted aerosol optical thickness (τ_{a550}^f) in each aerosol pixel was converted to aerosol column mass density (M_d g/m^2) as in (8)

$$M_d = \tau_{a550}^f / \beta_e \tag{8}$$

where β_e (expressed in square meters per gram) is the smoke aerosol specific extinction or mass extinction efficiency [2]. β_e, which is the sum of mass scattering efficiency (β_s) and mass absorption efficiency (β_a), can be obtained using various techniques, especially from *in situ* measurements. It has different ranges of values for different aerosol types (smoke, dust, pollution, sea salt), is wavelength dependent, and increases with relative humidity [2]. Reid *et al.* [36] published a detailed review of β_s and β_a, as well as other optical properties of smoke

aerosols based on measurement results from a large number of published works. Although β_s and β_a vary to a certain extent between ecosystem types, Reid *et al.* [36] found that at the 550-nm wavelength, β_s is in the range of 3–4 m^2/g for fresh ($\sim$5 min old) smoke and 4–4.3 m^2/g for aged (>1 h) smoke, while β_a has an overall range of 0.4–0.8 m^2/g. Since the smoke observed in the vicinity of fires by MODIS would be predominantly aged between 5 min and 1 h, we selected the median values from the above ranges, i.e., $\beta_s = 4$ and $\beta_a = 0.6$, which makes $\beta_e = 4.6$ m^2/g, for all analyses done in this paper. It is, however, noteworthy that aerosol and chemical transport models use values of β_e that are at least 50% higher than this [2], [37]. Also the 0.11 g/m^2 conversion factor proposed in [11] and [15] amounts to a β_e value of $\sim$9.1 m^2/g, which is close to the value of $\sim$8.4 m^2/g (from a conversion factor of 0.1188 g/m^2) (Shana Mattoo, personal communication, 2004) derived from aerosol models and used to generate the MODIS "Mass_Concentration_Land" product in a biomass-burning regime [33].

2) Wind Speed and Smoke Emission: Depending on their size and power, fires can inject smoke to altitudes varying from several meters to several kilometers before the force of injection gives way to the force of the wind. For the sizes of fires typically detectable by MODIS at 1-km resolution [15], it is estimated that the smoke injection height would be at least 0.5 km. Although the very large fires that occurred in Quebec in July 2002 were found to occasionally inject smoke to heights of up to 8 km [38], it is estimated that globally most fires would inject smoke to heights of <3 km. Therefore, for this study, we have adopted a global average injection height of 1.5 km for application of smoke transport in the vicinity of fires.

Using the zonal (u) and meridional (v) components of the wind vector at 850 mb atmospheric pressure (corresponding to an altitude of approximately 1.5 km) extracted from the NCEP/NCAR reanalysis dataset, the wind speed (WS) over each aerosol pixel was calculated as follows:

$$\mathrm{WS} = \sqrt{u^2 + v^2}. \tag{9}$$

Assuming that the ground pixel size is square and that the wind blows continuously in a linear fashion, for an aerosol pixel of area A^{ap}, the distance (L) over which the wind would blow in order to clear all existing aerosol in a pixel is assumed to be approximately

$$L = \sqrt{A^{\mathrm{ap}}}. \tag{10}$$

Although it would have been possible to calculate the distance across the pixel in the direction perpendicular to the wind direction, this would not necessarily increase the accuracy since the wind direction is not perfectly constant nor is the pixel orientation with respect to the wind perfectly regular. Therefore, the time (T^{ap}) it would take to clear all previously existing smoke aerosol from the pixel is

$$T^{\mathrm{ap}} = L/\mathrm{WS}. \tag{11}$$

This is assumed to be the time period during which the smoke within that aerosol pixel was emitted. It will be taken into consideration in deriving the smoke emission rates in the whole-fire-based calculations below.

B. Stage Two: Whole-Fire-Based Calculations

After the individual pixel-based calculations, the process of calculating emission rates advances to the stage of clustering all aerosol pixels constituting a fire or a set of fires observed by MODIS within a defined locale at the Terra or Aqua daytime overpass each day. All aerosol pixels containing fire within that locale are identified and counted, whether or not aerosol parameters are retrieved in those pixels, and the total number of these aerosol pixels containing fire may be denoted by N_{af}. The total fire radiative power (or energy per second) R_{fre} (in megawatts or megajoules per second) emitted by the fire cluster is calculated by summing all the subtotal radiative powers R^i_{fre} within each individual aerosol pixel

$$R_{\mathrm{fre}} = \sum_{i=1}^{N_{af}} R^i_{\mathrm{fre}}. \tag{12}$$

The total area (A_T) of the locale where the influence of the fire is being measured is considered to be the area of all the aerosol pixels containing fire. A_T is given by

$$A_T = \sum_{i=1}^{N_{af}} A_i^{\mathrm{ap}}. \tag{13}$$

The aerosol pixels actually containing aerosol retrievals (i.e., with AOT values) are counted and the total number is denoted by N_{aa}. Note that $N_{aa} \leq N_{af}$ because not all aerosol pixels containing fire had aerosol retrieval. N_{aa} is used to derive the average smoke emission per aerosol pixel, while N_{af} is used for calculations involving the total area of immediate fire influence in order to get an accurate estimation of the amount of smoke in the area.

The overall mean (M_D) of the aerosol mass density (M_d) for the fire is calculated as follows:

$$M_D = \left(\sum_{i=1}^{N_{aa}} (M_d)_i\right) / N_{aa}. \tag{14}$$

At this stage, the standard deviation (σ_{Md}) of M_d is also calculated, which when divided by M_D gives the standard error (ε_{Md}). The actual total mass of smoke aerosol M_{sa} emitted is the product of mean mass density (M_D) and total area (A_T)

$$M_{\mathrm{sa}} = M_D * A_T. \tag{15}$$

The average time period of emission of the smoke being measured is the mean of the periods for the individual aerosol pixels

$$T = \left(\sum_{i=1}^{N_{aa}} (T^{\mathrm{ap}})_i\right) \Big/ N_{aa}. \tag{16}$$

Finally, the rate of emission of smoke aerosol (or particulates) per unit time R_{sa} (in kilograms per second) is given by

$$R_{\mathrm{sa}} = M_{\mathrm{sa}}/T. \tag{17}$$

The standard error ($\varepsilon_{\mathrm{Rsa}}$) of R_{sa} is derived from ε_{Md} exactly the same way R_{sa} is derived from M_D using (15)–(17).

C. Stage Three: Derivation of FRE Coefficient of Smoke Emission (C_e)

From Section III, it is known that, for any given fire cluster or locale, fire radiative power (or fire radiative energy rate of release) R_{fre} derived directly from MODIS is expressed in megawatts or megajoules per second. From calculations in the earlier stages of this section, it is shown that the rate of emission of smoke particulates R_{sa} is expressed in (kilograms per second). Therefore, a plot of R_{sa} against R_{fre} will provide a convenient functional relationship to estimate the rate of emission of smoke particulates (R_{sa}) for any given fire radiative power (or radiative energy release rate) R_{fre} measured by MODIS.

MODIS-derived fire and aerosol data acquired throughout the year 2002, from both Terra and Aqua, were analyzed as described in the preceding sections for several regions of the world affected by fires. Table I shows the different regions selected for this study and their longitude and latitude boundaries. For each region, the daytime total smoke aerosol emission rate R_{sa} (in kilograms per second) was plotted against the daytime total FRE release rate R_{fre} (in megajoules per second) separately for Terra and Aqua overpasses. In each of the cases, the distribution of the scatter points showed that they were most favorably disposed to the fitting of zero-intercept regression lines (of the form $\mathrm{y} = \mathrm{mx}$, where $y = R_{\mathrm{sa}}, x = R_{\mathrm{fre}}$), although the degrees of correlation varied from region to region. Therefore, the gradient $m = C_e$. Hence, for any region with good fits, MODIS-measured R_{fre} only needs to be multiplied by C_e to derive the smoke emission rate R_{sa}, even in near real time.

V. Result Analysis

The following sections will describe the principal results of this work, the possible error sources, as well as qualitative comparison of the derived C_e values with corresponding literature values of emission factors for different ecosystems.

A. Regional FRE Coefficient of Smoke Emission (C_e)

Fig. 2 shows the scatter plots for six of the regions which produced good regression fits on plots of R_{sa} against R_{fre} for both Terra and Aqua, with coefficients of determination $r^2 > 0.65$ (i.e., correlation coefficient, $r > 0.8$). Among the rest of the regions whose plots are not shown, some showed similarly high correlation for both Terra and Aqua, others only for Terra or Aqua, and the rest did not produce high correlation for either. The possible sources of some of the uncertainties will be discussed below. It is noteworthy that, for each of the regions shown in Fig. 2, there is appreciable agreement between the values derived from Terra and Aqua, with the exception of Siberia.

Within each region, significant pixel clusters were identified as subregional zones, and similar plots were generated for them separately. In some cases, when the regional fit is good, fits for some zones within the region may not be as good, while excellent fits may be obtained for others. Fig. 3 shows the case of Canada, whose regional fit was excellent as shown in Fig. 2. The scatter plots in Fig. 3 show the three best fits obtained out of the zones in Canada. Whereas, the top right panel representing the southwestern part of Canada showed a very poor fit like those not shown, the two zones in the lower panels (representing northern Saskachewan and Ontario) gave outstanding fits. Even when the fit is not good for a parent region, certain zones within the region can produce excellent fits. Fig. 4 illustrates this phenomenon in the Asian region, for which the full regional fit gave very different slopes (i.e., C_e) of the regression lines for Terra and Aqua (Terra: $y = 0.037\times, r^2 = 0.415$; Aqua: $y = 0.061\times, r^2 = 0.728$), whereas for the individual zones shown, the C_e values from Terra and Aqua are appreciably close, with improved r^2. Most of the other Asian zones (plots not shown), however, did not give good fits. Another interesting example is the regional plot for the USA, which produced very poor fits (with $r^2 < 0.2$) for both Terra and Aqua. The zonal fits were much better, although they generally produced $r^2 < 0.6$. However, when a zone containing a known fire is plotted for the period of that specific fire, the correlation was excellent. Fig. 5 shows the pattern of fire occurrence for the U.S. in 2002 and scatter plot for the Biscuit fire, which occurred at the Oregon/California border during the month of August 2002. The correlations for Terra and Aqua are very high, even though their slopes are somewhat different due to some of the factors, which will be discussed in the next subsection.

B. Possible Error Sources

There are several possible sources of errors, which may have affected this work to various degrees in different regions. These errors have not all been explicitly quantified at this stage because the purpose of this paper is to demonstrate the feasibility of the technique for generating smoke emissions from FRE measurements. However, it is important to highlight the existence of these errors, and their effects will be quantified in future studies.

1) Simultaneous Observation of Fire and Emitted Smoke: The fire and aerosol data used for this study were observed simultaneously almost instantaneously at every pixel. However, it is a fact that the observed smoke was a cumulative sum of emissions over a finite period of time ending with the instant of observation. Since fire is dynamic, its state at the time of observation may have evolved during the period the bulk of smoke being measured was emitted. Nevertheless, at an average wind speed of 7 m/s, which is quite typical, most of the smoke observed over a 10-km resolution aerosol pixel would have been emitted within 12 min of the time of observation, during which time the intensity and size of a typical MODIS-scale fire may not have changed significantly. Furthermore, since there is practically equal likelihood of increase or decrease in the fire intensity during that time period, an error introduced by such a change is most likely random, and not biased. Therefore, although this simultaneous observation of fire and smoke could possibly introduce some error, it is believed that such errors would be insignificant in comparison with some of the other possible errors to be described in the following subsections.

2) Accuracy of MODIS Aerosol Optical Thickness: The MODIS aerosol optical thickness, from which the smoke aerosol emission rate R_{sa} was ultimately derived, is susceptible

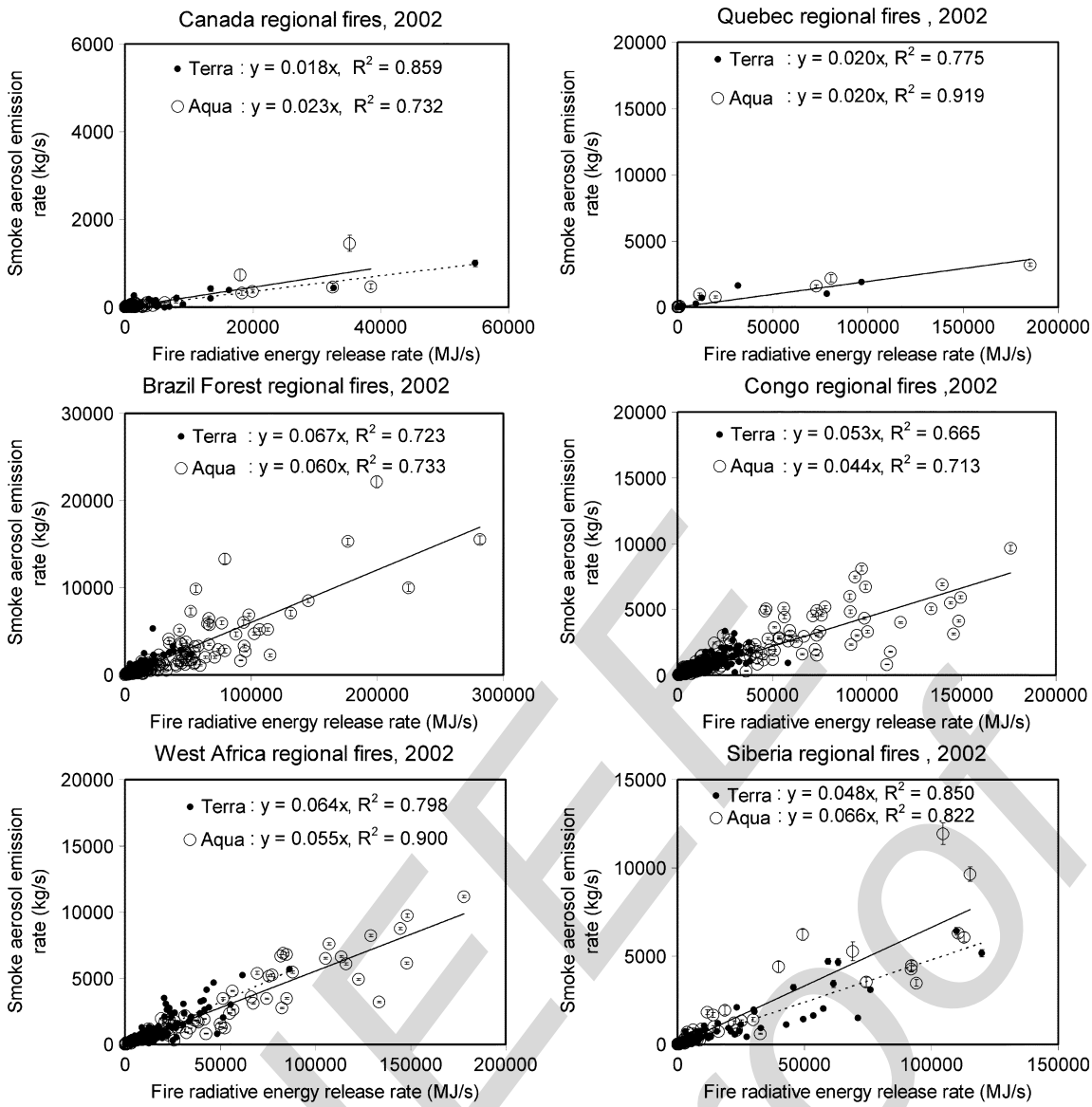

Fig. 2. Regional correlations between rates of emission of smoke aerosols $R_{\rm sa}$ (kilograms per second) and the rates of release of fire radiative energy $R_{\rm fre}$ (megajoules per second or megawatts) from fires detected by MODIS on (dots and dotted lines) Terra and (circles and solid lines) Aqua throughout the designated regions in 2002. Each data point represents one MODIS daytime overpass over the region. Vertical error bars represent the standard errors of $R_{\rm sa}$.

to errors from the aerosol retrieval processes and assumptions, as analyzed in the papers reporting the retrieval and validation of these aerosol products [39]–[43], [33]. In particular, AOT retrieved over land is found to be less accurate than retrievals over ocean due to several unfavorable factors, especially the influence of the land surface background. Nevertheless, only the over-land AOT data were used in this work in order to derive emissions directly above the fires, which are normally over land. Prior to the launch of MODIS, an investigation of the influence of smoke spatial variability on the accuracy of aerosol retrieval at 10-km resolution was conducted using the 50-m resolution MODIS Airborne Simulator (MAS) data over parts of Brazil, and the uncertainty was found to be within 10% for typical AOT values of 0.2 to 2.0 irrespective of distance from local sources [44]. Globally, the MODIS over-land AOT has an uncertainty range of $\pm(0.05 + 0.2\tau_{a\lambda})$ [39], although specific accuracy varies from region to region. A detailed comparison of both Terra and Aqua MODIS τ_{a550} against collocated ground-based Aerosol Robotic Network (AERONET) measurements acquired from 2000 to 2003 over land shows that MODIS currently overestimates AERONET by 10% to 50% in Asia, Europe, and North America, and by up to 100% in the Middle East and Australia. However, MODIS is accurate to within 10% of AERONET observations in southern Africa, Brazil, and Russia, but underestimates AERONET by 10% to 20% over West Africa [43]. Any AOT errors in the MODIS aerosol products used in this work must have propagated through the calculations done.

3) Conversion of AOT to Aerosol Mass Density: To derive the smoke aerosol mass emission rate, the AOT was first converted to smoke aerosol mass density (M_d g/m^2) by dividing with a constant mass extinction efficiency (β_e) value of 4.6 m^2/g derived from *in situ* measurements. However, as mentioned above, aerosol model-derived values for β_e range between 6 and 9 m^2/g [2], [11], [15], [37]. Given the difference in the measurement conditions, it is not obvious that the value

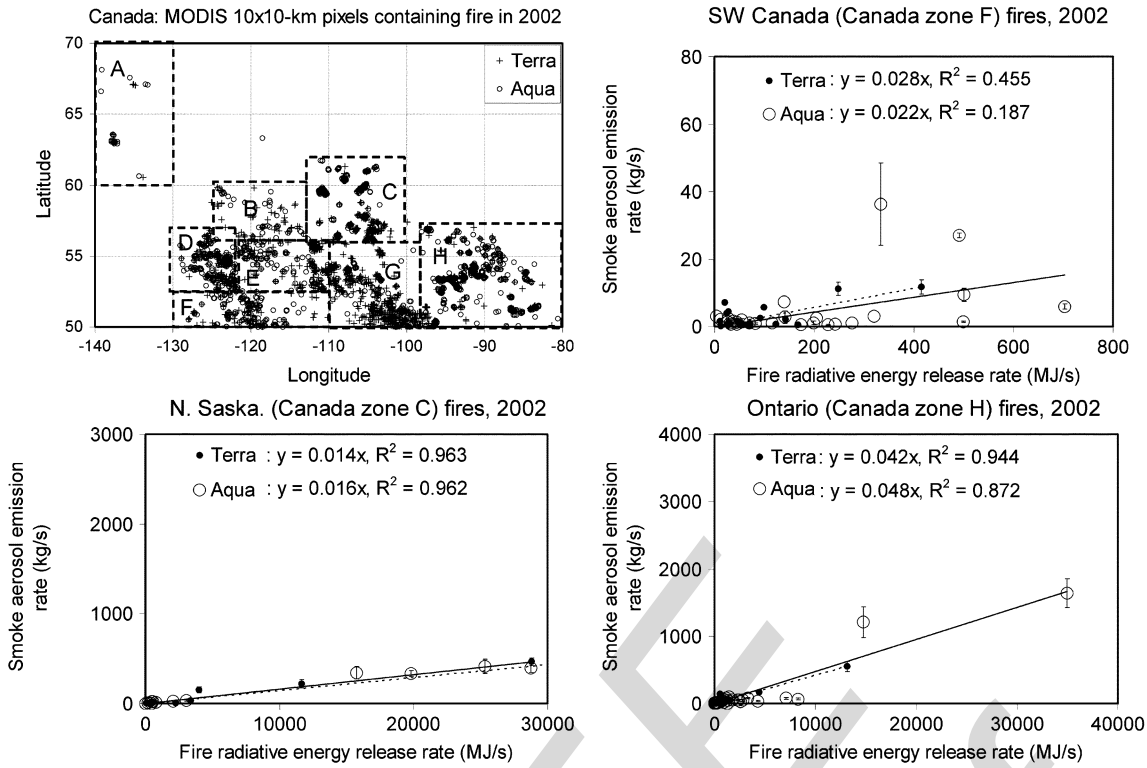

Fig. 3. (Top left panel) Canadian regional MODIS aerosol pixels containing fire as detected from (crosses) Terra and (circles) Aqua in 2002. Rectangular boxes are used to delineate zones with significant pixel clusters. Scatter plots [Terra (dots and dotted lines) and Aqua (circles and solid lines)] are shown for three zones with the highest correlations, demonstrating the zonal differences in the relationships between rate of emission of smoke aerosols $R_{\rm sa}$ (kilograms per second) and the rate of release of fire radiative energy $R_{\rm fre}$ (megajoules per second or megawatts). Each data point represents one MODIS daytime overpass over the region. Vertical error bars represent the standard errors of $R_{\rm sa}$.

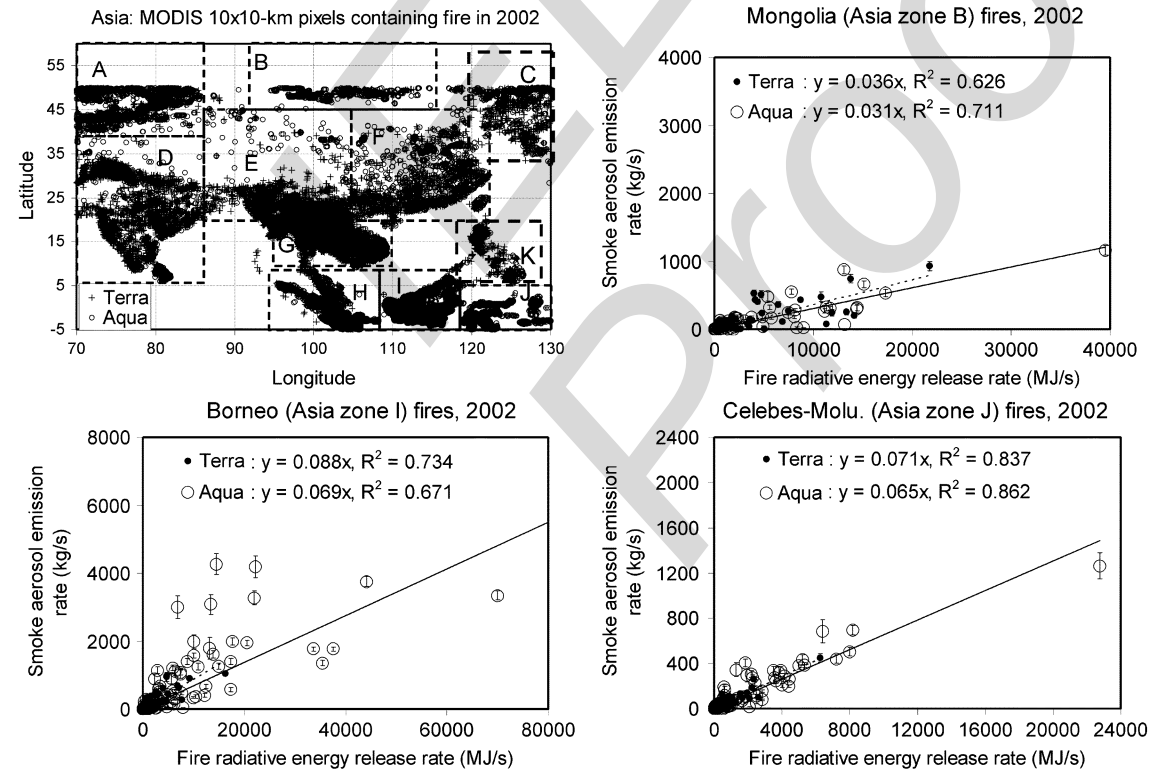

Fig. 4. (Top left panel) Asian regional MODIS aerosol pixels containing fire as detected from (crosses) Terra and (circles) Aqua in 2002. Rectangular boxes are used to delineate zones with significant pixel clusters. Scatter plots [Terra (dots and dotted lines) and Aqua (circles and solid lines)] are shown for three of the zones, each having very similar slopes or appreciably high correlation for Terra or Aqua or both, demonstrating the relationships between rate of emission of smoke aerosols $R_{\rm sa}$ (kilograms per second) and the rate of release of fire radiative energy $R_{\rm fre}$ (megajoules per second or megawatts). Each data point represents one MODIS daytime overpass over the region. Vertical error bars represent the standard errors of $R_{\rm sa}$.

based on *in situ* observations is the most appropriate for satellite applications. If the true satellite-appropriate value is anywhere between the *in situ* ($\beta_e = 4.6$) and model ($6 \leq \beta_e \leq 9$) values, then the $\beta_e = 4.6$ used in this work may have lead to a 0% to 100% overestimation of M_d, leading to the same level of overestimation in $R_{\rm sa}$. Furthermore, β_e typically increases with relative humidity (RH), although smoke is not very hygroscopic. Generally, at 80% RH the increase in smoke β_e is of the order of 10% to 35% and is much smaller at $\rm RH < 70\%$ [2], [18]. Since over 95% of the data used in this study were measured at $\rm RH < 70\%$, with regional RH averages ranging between 35% and 65%, and because of the current uncertainties in smoke hygroscopicity measurements (as discussed in [18]), β_e was not corrected for RH in this work. If RH correction had been applied to β_e, it would have been larger by 5% to 25%, which would have reduced the values of $R_{\rm sa}$ computed with it by the same margin. Therefore, the emission rates $R_{\rm sa}$ derived in this work may have been overestimated by 5% to 25% due to smoke aerosol hygroscopicity. Also, it is recognized that the value of β_e varies between ecosystems and regions, although a constant value of $\beta_e = 4.6$ was used globally in this work for convenience, since it was not easy to resolve all the differences (regional, ecosystem, smoke age, humidification, and hygroscopicity). In addition, the choice of AOT at the 550-nm wavelength is not necessarily ideal. This wavelength was chosen because it coincides with the central part of the visible portion of the electromagnetic spectrum, and is the most frequently used wavelength in aerosol radiation studies.

4) Accuracy of NCEP Wind Fields: The smoke aerosol emission rate $R_{\rm sa}$ was derived from the smoke aerosol mass density M_d using assimilated wind fields obtained from the NCEP/NCAR reanalysis dataset [34] at a 1° spatial resolution. Since the reanalysis data were assimilated from a wide variety of sources, including measurements from the ground, ship, buoys, balloons, aircraft, and satellites, their accuracy would depend on the measurement techniques, conditions, and sampling density. Therefore, wind data over regions with sparse measurement coverage and less advanced instrumentation and techniques, such as certain parts of Africa and Asia, are expected to be less accurate. In addition to the potential intrinsic inaccuracies in the wind vectors, it is noteworthy also that their 1° spatial resolution is ten times coarser than the 10-km resolution of the MODIS aerosol product upon which the smoke emission rate calculations are based. Also, the NCEP/NCAR reanalysis data were only available at 6-h intervals: 0h, 6h, 12h, 18h UTC. Therefore, for each MODIS observation the wind fields closest in time were used, amounting to a time difference of up to 3 h. However, since any change in wind speed can be either increase or decrease, any discrepancy caused by this change would be random, and not biased. Nevertheless, all the foregoing factors would most likely affect the accuracy of the calculations done in this paper, although the effect is not easily quantifiable.

5) Smoke Plume Height Assumption: The smoke aerosol emission rate $R_{\rm sa}$ was derived based on wind vectors at 850-mb pressure level. By basing the calculations on this pressure level, which corresponds to an altitude of approximately 1.5 km, it is assumed that, at this height, the vertical force of injection of the smoke by the fire would give way to the horizontal force of the wind. Because of the variation of fire sizes and strengths as well as topography across the world, this assumed pressure level or elevation may not be the applicable smoke-dispersion altitude in certain areas of the world. Any area where the effective smoke plume height does not correspond to this pressure level may be adversely affected. In future work, Lidar measurements can be used to determine the smoke plume heights more accurately. However, to assess the sensitivity of $R_{\rm sa}$ to winds at different pressure levels, $R_{\rm sa}$ was also derived with wind vectors at 925 mb ($\sim$0.75 km height) and 700 mb ($\sim$3 km height) and used to compute C_e to compare with values computed with 850-mb winds. The difference in the results is variable, but small in most of the regions, as will be discussed in a later section.

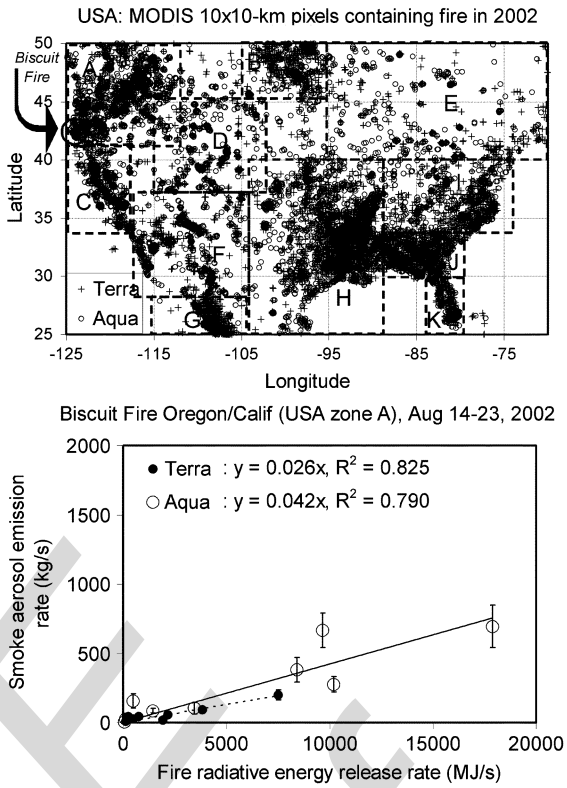

Fig. 5. U.S. fires. (Top panel) MODIS aerosol pixels containing fire as detected from (crosses) Terra and (circles) Aqua in 2002. Rectangular boxes are used to arbitrarily delineate zones with significant pixel clusters. The subzonal cluster representing the Biscuit fire, which burned in the Oregon/California border in August 2002 is encircled. (Bottom panel) Scatter plots [Terra (dots and dotted lines) and Aqua (circles and solid lines)] for zone A for the period of August 14–23, 2002, corresponding to the time of the main event of the Biscuit fire, show the relationships between the rate of emission of smoke aerosols $R_{\rm sa}$ (kilograms per second) and the rate of release of fire radiative energy $R_{\rm fre}$ (megajoules per second or megawatts). Each data point represents one MODIS daytime overpass over zone A. Vertical error bars represent the standard errors of $R_{\rm sa}$. Notice the very high correlation for both Terra and Aqua.

6) Accuracy and Consistency of MODIS-Derived $R_{\rm fre}$: The MODIS-derived fire radiative energy release rate $R_{\rm fre}$ was not yet validated at the time of this study. This is because, although it is possible to validate fire locations, the validation of the actual radiative energy released is somewhat complex. Effort is underway to conduct experiments for its validation. Therefore, like all products derived through the process of remote sensing, this parameter is likely to contain some inaccuracies. However,

Wooster *et al.* [45] compared MODIS-derived $R_{\rm fre}$ with that derived using a different approach from the Bi-spectral Infrared Detection (BIRD) small satellite designed mainly for fire and other hotspot sensing, and found that the two sensors agreed to within 15% of each other, although for smaller fires, MODIS (1-km resolution) was found to underestimate $R_{\rm fre}$ by up to 46% with respect to BIRD (370-m resolution). Nevertheless, the medium to large fires measured by MODIS are believed to be responsible for most of the global smoke emissions [15]. In any case, since the MODIS AOT products are validated and are used in conjunction with $R_{\rm fre}$ for the derivation of C_e in this work, any perceived accuracy for the derived C_e can serve as some form of validation for $R_{\rm fre}$.

7) Cloud Cover: Cloud cover is a ubiquitous phenomenon affecting the accuracy of the remote sensing of surface or other atmospheric features in a complex fashion. For instance, whereas cloud effect lowers the capacity for fire detection, it increases the potential for overestimation of aerosol loading. Simply put, the more the cloud effect, the less the fire detected, and the more the amount of smoke assumed present; thereby drastically reducing the correlation between $R_{\rm sa}$ and $R_{\rm fre}$, and contaminating the resulting C_e. The effect of cloud cover in the calculations performed in this work is not easily quantifiable, although it is not likely to be very significant, since the pixel-level processing involved the matching of fire and aerosol pixels measured at the same time under "cloud-free" conditions, leaving only possible residual cloud contamination.

8) Heterogeneity of Regional/Zonal Characteristics: A particular region, zone, or even a small area being studied as a unit may be very inhomogeneous in terms of ecosystem type, fuel load and moisture, fire sizes, and the relative smoldering to flaming ratio across the landscape and seasons. This spatial and temporal heterogeneity can affect the relationship between $R_{\rm sa}$ and $R_{\rm fre}$ as well as the accuracy of the derived C_e. In particular, a fire with a given $R_{\rm fre}$ can produce a much higher $R_{\rm sa}$ when smoldering than when flaming. However, it is believed that most biomass fires comprise a mixture of flaming and smoldering constituents, with only very few in either extreme. The pixel-cluster-based analysis and scatter plots used in computing C_e would dampen the effect of any discrepancy between smoldering and flaming emissions.

It is also important to highlight that data acquired only at Terra and Aqua daytime overpasses (only two samples), as used in this work, may not have accounted for the diurnal cycle of fires adequately. However, different fires within the same area start at different times of day and may be at different stages of burn when captured by MODIS, thereby providing a certain variety in the fire-cycle representation. It is hoped that, in future, data from geostationary satellites such as the Geostationary Operational Environmental Satellites (GOES) [16] would be incorporated into this type of analysis in order to improve the representation of fire diurnal life cycle.

C. Derived Emission Coefficients (C_e) and Ecosystem Types

As mentioned in the introduction, Andreae and Merlet [6] compiled the average values of traditionally derived emission factors reported in the literature for fire-emitted smoke aerosols and numerous trace-gas species across a number of ecosystem types. The average emission factors (EF_x) for smoke total particulate matter (TPM) for different ecosystems may be used as a reference to qualitatively verify whether the values computed in this work from satellite measurements are reasonable.

In this study, the regions or subregional zones were not selected on the basis of ecosystem boundaries, but on the basis of geographical convenience and pixel clustering. However, it is possible to identify the dominant ecosystem for each region or zone. Fig. 6 shows the rough rectangular boundaries of the selected regions and zones delineated on a global ecosystem map. The ecosystem categories are based on the classification scheme adopted by the International Geosphere-Biosphere Program (IGBP).

Fig. 7 shows plots of C_e values computed for each of the regions or zones using wind vectors at 850 mb ($\sim$1.5 km), which is the adopted smoke dispersion height for this study, coplotted with C_e at 925 mb ($\sim$0.75 km) and 700 mb ($\sim$3 km) for comparison. For most of the regions, the higher or lower level winds did not make much difference, but the difference was quite substantial for a few regions such as Zambia, southern Russia, and the southeast Asian zones of Borneo and the Philippines, particularly with the higher level winds (700 mb), which for Borneo produced a disproportionate C_e value of 0.16 that fell outside the plotting area. The regions are grouped according to the ecosystem categories presented in [6], based on their apparent dominant landcover types, as determined visually from the map in Fig. 6. The last group of regions (Europe, E_Kazakhstan, Mongolia, and the Philippines) is designated as "unclassified" because it was not obvious to determine their dominant ecosystem types. Only regions or zones whose C_e values at 850 mb from Terra or Aqua were appreciably close (with one not exceeding the other by more than 60%) and have a good Terra and Aqua average correlation ($r^2 > 0.6$) are plotted. The final average for each qualifying region or zone, at each pressure level (850, 925, 700 mb), was the weighted mean of C_e from Terra and Aqua, using their respective r^2 values as the weighting factors. Incidentally, most of the regions or zones that meet these accuracy thresholds are those whose ecosystem type is fairly homogeneous, and over which smoke is typically the dominant aerosol type (except for Europe). In the case of West Africa, where both smoke and dust occur quite considerably, in the 2002 data used for this study, over 95% of the fires occurred between October and February, which is the fire season when smoke is the dominant aerosol type, before the onset of the dust season (which usually starts in late January).

The superimposed thick horizontal bars in Fig. 7 are plots of the average literature values of emission factors [6], with their respective associated uncertainties plotted as error bars. Although the MODIS-derived C_e values cannot be quantitatively compared with the literature EF_x values, one positive generalization that can be made is that they vary with the different ecosystem types in the same manner. The exception is the extra-tropical forest type whose literature EF_x value is higher than those of the other ecosystems, whereas MODIS C_e values have the opposite trend. This could be because the data classified under "extratropical forest" in [6] may represent a broad range of ecosystem types, or may not even include data from boreal forests to which Alaska, Canada, Quebec, and Siberia belong.

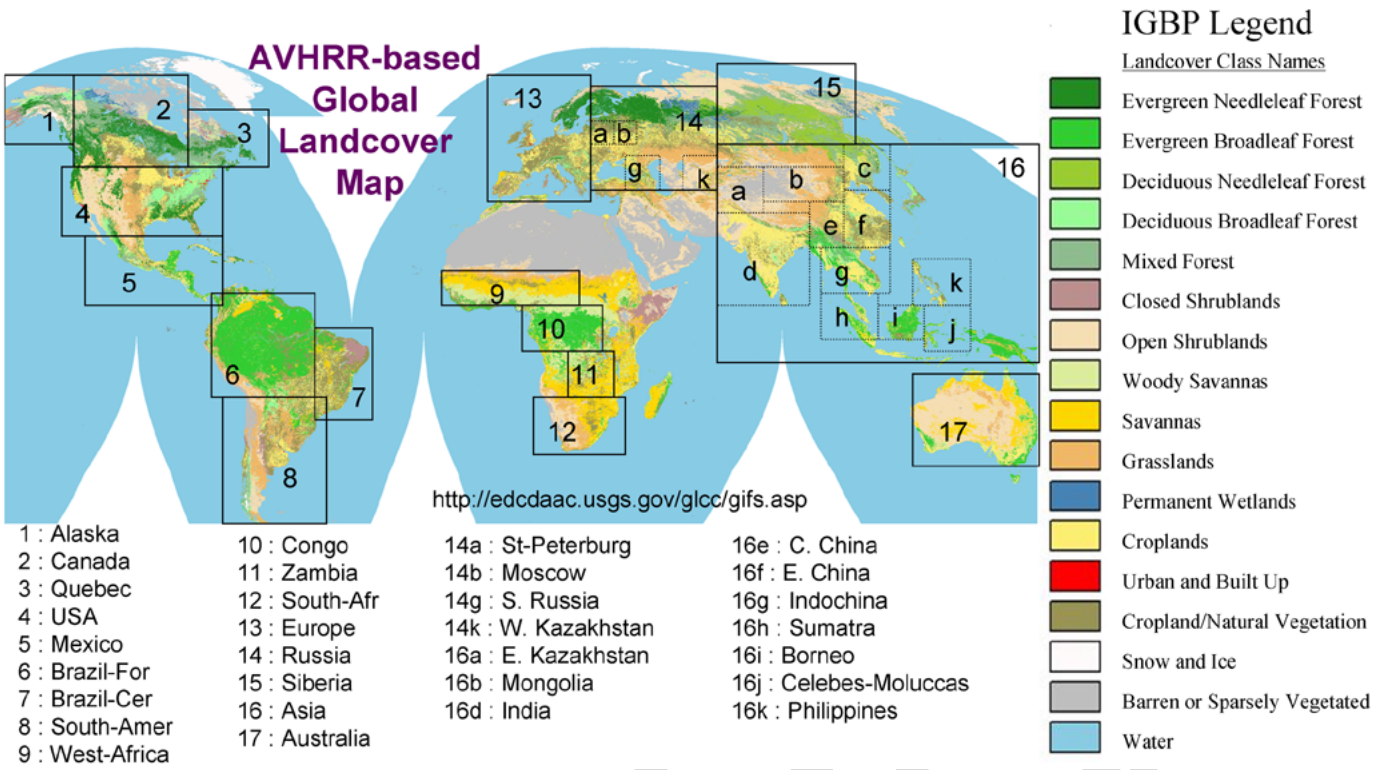

Fig. 6. Global landcover map generated by the U.S. Geological Survey in collaboration with other organizations, based on the Advanced Very High Resolution Radiometer data (April 1992 to March 1993), showing some of the main ecosystem categories according to the scheme adopted by the IGBP. The map was taken from the NASA land processes Distributed Active Archive Center web site (http://edcdaac.usgs.gov/glcc/gifs.asp). The regions selected for this study are delineated by solid-line rectangular boxes numbered from 1–17. Within each region, some of the subregional zones used in this study are enclosed with broken-line rectangular boxes labeled with alphabets (a–z), although not all the subregional zones studied are shown.

In this work, the MODIS-derived C_e values for Alaska, Canada, and Quebec are practically equal, thereby indicating appreciable consistency. The difference between these North American regions and Siberia may be a reflection of the differences in fire intensities between the boreal forests in the two continents [46]. Although the rest of the Russian sites are all grouped under agricultural residues, which is the designation used in [6], it is noteworthy that in the IGBP classification (Fig. 6), these zones include mostly areas designated as "cropland/natural vegetation." Therefore, their high C_e values also reflect the signal from peat fires associated with concentrated smoke emissions, which normally burn around Moscow and surrounding regions. The unclassified group could not be placed under any specific ecosystem type. The Philippines shows the highest C_e value among all plotted regions. Table II lists the C_e values derived with 850-mb wind fields. These values may be used for emission estimation with MODIS FRE measurements in their respective regions with caution, because the values have not been verified by other methods. Based on the perceived impacts of the error sources described above, the average uncertainty in the C_e values derived in this work is estimated to be of the order of $\pm 50\%$, with overestimation being more likely. However, the magnitude of the uncertainty is comparable to that currently estimated for the traditional methods [6], although this satellite technique has great potential for improvement in future research, when most of the potential errors would have been properly evaluated and accounted for in the calculations.

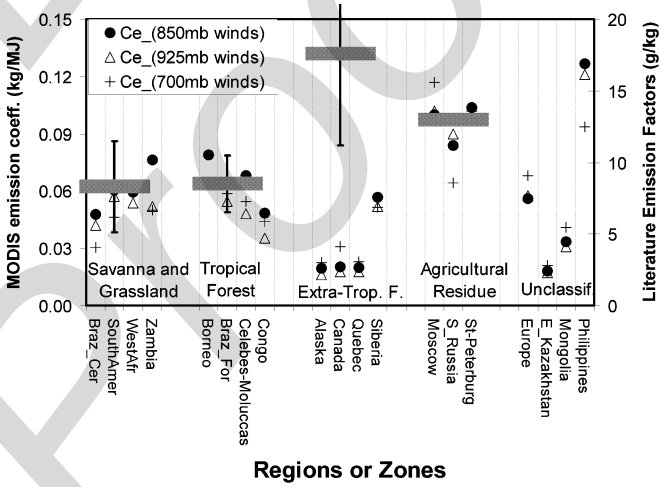

Fig. 7. FRE coefficients of emission (C_e) of smoke aerosol (scale on left vertical axis), derived with wind speeds at 850 mb (approximately 1.5-km altitude), are shown for various regions or zones alongside those derived with winds at 925 mb (~ 0.75 km) and 700 mb (~ 3 km). The different regions have been grouped according to the ecosystem categories of Andreae and Merlet [6], based on the dominant ecosystem type as visually determined from the land-cover map in Fig. 6. It was not obvious to determine the dominant ecosystem types for the last group designated as unclassified (Europe, E_Kazakhstan, Mongolia, and Philippines). Thick horizontal bars (scale on right vertical axis) represent the average literature values of traditionally derived emission factors (with associated error bars) for each of the ecosystem types [6].

TABLE II
ESTIMATES OF REGIONAL FRE-BASED SMOKE AEROSOL EMISSION COEFFICIENTS (C_e) FROM MODIS (BASED ON 850-mb WIND FIELDS)

Region	Description	PM emission coefficients (m^{-2} g)
	Savanna and Grassland Regions	
Braz_Cer	Brazil Cerrado savanna region	0.048
SouthAmer	South America below 20°S	0.061
WestAfr	West Africa	0.059
Zambia	Zambia in southern Africa	0.076
	Tropical Forest Regions	
Borneo	Borneo Island of Indonesia	0.079
Braz_For	Brazil topical forest region	0.063
Celebes-Moluccas	Celebes Molucas Island, Indonesia	0.068
Congo	Congo tropical forest, Africa	0.048
	Boreal Forest Regions	
Alaska	Alaska	0.020
Canada	Canada below 70°N (excluding Quebec)	0.020
Quebec	Quebec and Eastern Ontario	0.020
Siberia	Siberia North of 60°N	0.057
	Cropland/Natural Vegetation Regions	
Moscow	Moscow and environs	0.100
S_Russia	Southern Russia	0.084
St-Peterburg	St Peterburg and environs	0.104
	Unclassified	
Europe	Europe (excluding Russia)	0.056
E_Kazakhstan	East Kazakhstan	0.018
Mongolia	Mongolia	0.033
Philippines	The philippines	0.127

VI. CONCLUSION

This study has enabled the leveraging of satellite (and specifically MODIS) fire radiative energy measurements for use in emissions estimation. Emission coefficients C_e were derived for a number of regions, only for smoke aerosols, based on one-year's worth of data from MODIS. However, the same procedure can be used to derive similar coefficients for CO as well as for a number of other gases measurable from satellite.

Although C_e can be used to derive emissions from fire radiative energy measurements in all circumstances, there are areas of application that are particularly interesting as far as satellite remote sensing is concerned. The most important significance of the emission coefficients C_e derived in this work is that it can now enable the quantitative estimation of the emission of smoke directly and exclusively from satellite-derived $R_{\rm fre}$. It saves one the trouble of trying to quantify the total above-ground biomass, its moisture conditions, and fraction burned, as required in the traditional methods, which are complex processes prone to significant errors, and impossible to do in near real-time. It is also noteworthy that although satellite sensors measure aerosols (including smoke) only during the daytime, $R_{\rm fre}$ is measured both day and night. Therefore, when the accurate C_e value of an area is known, the rate of smoke emission from fires can be quantified day and night. This is a unique feature of the technique developed here.

One of the most attractive direct application areas can be in the (near) real-time monitoring of smoke emissions from fires. Although MODIS stores data onboard like many other sensors for later download when passing over designated receiving stations, nevertheless, it also broadcasts the raw data it collects immediately for direct reception by any listening ground-based station below it. This special feature of MODIS is referred to as Direct Broadcast (DB) of the data. Therefore, data can be received in real time at stations equipped with the DB receiving system. A large number of organizations currently possess this facility. Indeed, at the time of writing this paper, it is estimated that there are over 100 DB receiver systems worldwide. Experience shows that DB data can be downloaded and $R_{\rm fre}$ derived in less than 1 h (Wei Min Hao, personal communication, 2004). This implies that rate of emission of smoke $R_{\rm sa}$ can be derived in near real time, as soon as the satellite data are received and processed. As such, the concentration and spread of the smoke can be forecasted in true quantitative terms for neighboring regions days ahead of time, thereby enabling rapid advance decision-making for areas to be affected regarding possible alerts, warnings, shutdowns, or evacuations.

Another important significance of C_e is that it facilitates the direct ingestion of satellite fire data into smoke-emission, chemical-transport, and climate models. This will provide an alternative way of making accurate inventory of smoke emissions from different ecosystems, enabling models to run with minimal dependence on the knowledge of fuel loading, fuel moisture, and such other parameters conventionally used for emissions estimation in models.

ACKNOWLEDGMENT

The authors would like to thank the various MODIS science and support teams for the production and distribution of the MODIS data. Special thanks to M. Nishihama for providing the formulas for modeling the MODIS pixel-size variation, and to B. Ridgway for help with high volume data management. The authors are particularly grateful to the MODIS fire and aerosol groups for close collaboration and support, as well as for providing vital ideas and assistance during the development of this project. The authors also thank M. Wooster for many helpful discussions on fire radiative energy measurements. Appreciation also goes to J. Reid and an anonymous reviewer, who provided valuable comments and suggestions for improving the quality of the manuscript.

REFERENCES

[1] M. Scholes and M. O. Andreae, "Biogenic and pyrogenic emissions from Africa and their impact on the global atmosphere," *Ambio*, vol. 29, pp. 23–29, 2000.

[2] M. Chin, P. Ginoux, S. Kinne, O. Torres, B. N. Holben, B. N. Duncan, R. V. Martin, J. A. Logan, A. Higurashi, and T. Nakajima, "Tropospheric aerosol optical thickness from the GOCART model and comparisons with satellite and sun photometer measurements," *J. Atmos. Sci.*, vol. 59, pp. 461–483, 2002.

[3] Z. Li, S. Nadon, and J. Cihlar, "Satellite-based detection of Canadian boreal forest fires: Development and application of the algorithm," *Int. J. Remote Sens.*, vol. 21, no. 16, pp. 3057–3069, 2000.

[4] IPCC, "Third Assessment Report (TAR), Climate Change 2001, the Scientific Basis, Contribution of Working Group I to the Third Assessment Report of the International Panel on Climate Change," Cambridge Univ. Press, New York, J. T. Houghton *et al.*, Ed., 2001.

[5] P. M. Fearnside, "Global warming and tropical land-use change: Greenhouse gas emissions from biomass burning, decomposition and soils in forest conversion, shifting cultivation and secondary vegetation," *Clim. Change*, vol. 46, no. 1–2, pp. 115–158, 2000.

[6] M. O. Andreae and P. Merlet, "Emission of trace gases and aerosols from biomass burning," *Global Biogeochem. Cycles*, vol. 15, pp. 955–966, 2001.

[7] W. Seiler and P. J. Crutzen, "Estimates of gross and net fluxes of carbon between the biosphere and the atmosphere from biomass burning," *Clim. Change*, vol. 2, pp. 207–248, 1980.

[8] P. J. Crutzen and M. O. Andreae, "Biomass burning in the tropics: Impact on atmospheric chemistry and biogeochemical cycles," *Science*, vol. 250, pp. 1669–1678, 1990.

[9] M. O. Andreae, "Biomass burning: Its history, use, and distribution and its impact on environmental quality and global climate," in *Global Biomass Burning: Atmospheric, Climatic, and Biospheric Implications*, J. S. Levine, Ed. Cambridge, MA: MIT Press, 1991, pp. 3–21.

[10] W. M. Hao and M.-H. Liu, "Spatial and temporal distribution of tropical biomass burning," *Global Biogeochem. Cycles*, vol. 8, pp. 495–503, 1994.

[11] Y. J. Kaufman, C. J. Tucker, and I. Fung, "Remote sensing of biomass burning in the tropics," *J. Geophys. Res.*, vol. 95, pp. 9927–9939, 1990.

[12] E. M. Prins and W. P. Menzel, "Geostationary satellite detection of biomass burning in South America," *Int. J. Remote Sens.*, vol. 13, pp. 2783–2799, 1992.

[13] C. O. Justice, J. D. Kendall, P. R. Dowty, and R. J. Scholes, "Satellite remote sensing of fires during the SAFARI campaign using NOAA AVHRR data," *J. Geophys. Res.*, vol. 101, pp. 23 851–23 863, 1996.

[14] W. P. Menzel and E. M. Prins, "Monitoring biomass burning with the new generation of geostationary satellites," in *Biomass Burning and Global Change*, J. S. Levine, Ed. Cambridge, MA: The MIT Press, 1996, pp. 56–64.

[15] Y. J. Kaufman, C. O. Justice, L. P. Flynn, J. D. Kendall, E. M. Prins, L. Giglio, D. E. Ward, W. P. Menzel, and A. W. Setzer, "Potential global fire monitoring from EOS-MODIS," *J. Geophys. Res.*, vol. 103, pp. 32215–32 238, 1998.

[16] E. M. Prins, J. M. Feltz, W. P. Menzel, and D. E. Ward, "An overview of GOES-8 diurnal fire and smoke results for SCAR-B and 1995 fire season in South America," *J. Geophys. Res.*, vol. 103, no. D24, pp. 31 821–31 835, 1998.

[17] B. N. Duncan, R. V. Martin, A. C. Staudt, R. Yevich, and J. A. Logan, "Interannual and seasonal variability of biomass burning emissions constrained by satellite observations," *J. Geophys. Res.*, vol. 108, no. D2, 4100, 2003. DOI: 10.1029/2002JD002378.

[18] J. S. Reid, E. M. Prins, D. L. Westphal, C. C. Schmidt, K. A. Richardson, S. A. Christopher, T. F. Eck, E. A. Reid, C. A. Curtis, and J. P. Hoffman, "Real-time monitoring of South American smoke particle emissions and transport using a coupled remote sensing/box-model approach," *Geophys. Res. Lett.*, vol. 31, no. L06107, 2004. DOI: 10.1029/2003GL018845.

[19] J. J. Hoelzemann, M. G. Schultz, G. P. Brasseur, C. Granier, and M. Simon, "Global wildland fire emission model (GWEM): Evaluating the use of global area burnt satellite data," *J. Geophys. Res.*, vol. 109, no. D14S04, 2004. DOI: 10.1029/2003JD003666.

[20] A. Ito and J. E. Penner, "Global estimates of biomass burning emissions based on satellite imagery for the year 2000," *J. Geophys. Res.*, vol. 109, no. D14S05, 2004. DOI: 10.1029/2003JD004423.

[21] E. S. Kasischke and J. E. Penner, "Improving global estimates of atmospheric emissions from biomass burning," *J. Geophys. Res.*, vol. 109, no. D14S01, 2004. DOI: 10.1029/2004JD004972.

[22] A. Palacios-Orueta, A. Parra, E. Chuvieco, and C. Carmona-Moreno, "Remote sensing and geographic information systems methods for global spatiotemporal modeling of biomass burning emissions: Assessment in the African continent," *J. Geophys. Res.*, vol. 109, no. D14S09, 2004. DOI: 10.1029/2004JD004734.

[23] M. Simon, S. Plummer, F. Fierens, J. J. Hoelzemann, and O. Arino, "Burnt area detection at global scale using ATSR-2: The GLOBSCAR products and their qualification," *J. Geophys. Res.*, vol. 109, no. D14S02, 2004. DOI: 10.1029/2003JD003622.

[24] K. Tansey *et al.*, "Vegetation burning in the year 2000: Global burned area estimates from SPOT VEGETATION data," *J. Geophys. Res.*, vol. 109, no. D14S03, 2004. DOI: 10.1029/2003JD003598.

[25] D. P. Roy, P. E. Lewis, and C. O. Justice, "Burned area mapping using multitemporal moderate spatial resolution data—A bi-directional reflectance model-based expectation," *Remote Sens. Environ.*, vol. 83, pp. 263–286, 2002.

[26] R.-R. Li, Y. J. Kaufman, W. M. Hao, J. M. Salmon, and B.-C. Gao, "A technique for detecting burn scars using MODIS data," *IEEE Trans. Geosci. Remote Sens.*, vol. 42, no. 6, pp. 1300–1308, Jun. 2004.

[27] S. Korontzi, D. P. Roy, C. O. Justice, and D. E. Ward, "Modeling and sensitivity analysis of fire emissions in southern Africa during SAFARI 2000," *Remote Sens. Environ.*, vol. 92, pp. 255–275, 2004.

[28] E. Chuvieco, D. Cocero, I. Aguado, A. Palacios, and E. Prado, "Improving burning efficiency estimates through satellite assessment of fuel moisture content," *J. Geophys. Res.*, vol. 109, no. D14S07, 2004. DOI: 10.1029/2003JD003467.

[29] Y. J. Kaufman, C. Ichoku, L. Giglio, S. Korontzi, D. A. Chu, W. M. Hao, R.-R. Li, and C. O. Justice, "Fires and smoke observed from the earth observing system MODIS instrument—Products, validation, and operational use," *Int. J. Remote Sens.*, vol. 24, no. 8, pp. 1765–1781, 2003.

[30] C. O. Justice, L. Giglio, S. Korontzi, J. Owens, J. T. Morisette, D. Roy, J. Descloitres, S. Alleaume, F. Petitcolin, and Y. Kaufman, "The MODIS fire products," *Remote Sens. Environ.*, vol. 83, no. 1–2, pp. 244–262, 2002.

[31] M. J. Wooster, "Small-scale experimental testing of fire radiative energy for quantifying mass combusted in natural vegetation fires," *Geophys. Res. Lett.*, vol. 29, no. 21, 2002. DOI: 10.1029/2002GL015487.

[32] L. Giglio, J. Descloitres, C. O. Justice, and Y. J. Kaufman, "An enhanced contextual fire detection algorithm for MODIS," *Remote Sens. Environ.*, vol. 87, pp. 273–282, 2003.

[33] L. A. Remer, Y. J. Kaufman, D. Tanre, S. Mattoo, D. A. Chu, J. V. Martins, R.-R. Li, C. Ichoku, R. C. Levy, R. G. Kleidman, T. F. Eck, E. Vermote, and B. N. Holben, "The MODIS aerosol algorithm, products, and validation," *J. Atmos. Sci.*, vol. 62, pp. 947–973, 2005.

[34] E. Kalnay, M. Kanamitsu, R. Kistler, W. Collins, D. Deaven, L. Gandin, M. Iredell, S. Saha, C. White, J. Woollen, Y. Zhu, M. Chelliah, W. Ebisuzaki, W. Higgins, J. Janowiak, K. C. Mo, C. Ropelewski, J. Wang, A. Leetmaa, R. Reynolds, R. Jenne, and D. Joseph, "The NCEP/NCAR 40-year reanalysis project," *Bull. Amer. Meteorol. Soc.*, vol. 77, no. 3, pp. 437–71, 1996.

[35] M. Nishihama, R. Wolfe, D. Solomon, F. Patt, J. Blanchette, A. Fleig, and E. Masuoka, "MODIS Level 1A Earth Location: Algorithm Theoretical Basis Document Version 3.0," NASA Goddard Space Flight Center, Greenbelt, MD, MODIS Technical Report Series, NASA Tech. Memo. 104594, Vol. 2, May 1997.

[36] J. S. Reid, T. F. Eck, S. A. Christopher, R. Koppmann, O. Dubovik, D. P. Eleuterio, B. N. Holben, E. A. Reid, and J. Zhang, "A review of biomass burning emissions part III: Intensive optical properties of biomass burning particles," *Atmos. Chem. Phys. Discuss.*, vol. 4, pp. 5201–5260, 2004.

[37] S. Kinne, U. Lohmann, J. Feichter, M. Schulz, C. Timmreck, S. Ghan, R. Easter, M. Chin, P. Ginoux, T. Takemura, I. Tegen, D. Koch, M. Herzog, J. Penner, G. Pitari, B. Holben, T. Eck, A. Smirnov, O. Dubovik, I. Slutsker, D. Tanre, O. Torres, M. Mishchenko, I. Geogdzhayev, D. A. Chu, and Y. Kaufman, "Monthly averages of aerosol properties: A global comparison among models, satellite data, and AERONET ground data," *J. Geophys. Res.*, vol. 108, no. D20, 4634, 2003. DOI: 10.1029/2001JD001253.

[38] P. R. Colarco, M. R. Schoeberl, B. G. Doddridge, L. T. Marufu, O. Torres, and E. J. Welton, "Transport of smoke from Canadian forest fires to the surface near Washington, D.C.: Injection height, entrainment, and optical properties," *J. Geophys. Res.*, vol. 109, no. D06203, 2004. DOI:10.1029/2003JD004248.

[39] D. A. Chu, Y. J. Kaufman, C. Ichoku, L. A. Remer, D. Tanré, and B. N. Holben, "Validation of MODIS aerosol optical depth retrieval over land," *Geophys. Res. Lett.*, vol. 29, no. 12, Jun. 29, 2002. DOI; 10.1029/2001GL013205.

[40] C. Ichoku, D. A. Chu, S. Mattoo, Y. J. Kaufman, L. A. Remer, D. Tanré, I. Slutsker, and B. Holben, "A spatio-temporal approach for global validation and analysis of MODIS aerosol products," *Geophys. Res. Lett.*, vol. 29, no. 12, Jun. 29, 2002. DOI: 10.1029/2001GL013206.

[41] L. A. Remer, D. Tanré, Y. J. Kaufman, C. Ichoku, S. Mattoo, R. Levy, D. A. Chu, B. N. Holben, O. Dubovik, Z. Ahmad, A. Smirnov, J. V. Martins, and R.-R. Li, "Validation of MODIS aerosol retrieval over ocean," *Geophys. Res. Lett.*, vol. 29, no. 12, Jun. 29, 2002. DOI: 10.1029/2001GL013204.

[42] C. Ichoku, L. A. Remer, Y. J. Kaufman, R. Levy, D. A. Chu, D. Tanre, and B. N. Holben, "MODIS observation of aerosols and estimation of aerosol radiative forcing over southern africa during SAFARI 2000," *J. Geophys. Res.*, vol. 108, no. D13, 8499, 2003. DOI: 10.1029/2002JD002366.

[43] C. Ichoku, L. A. Remer, and T. F. Eck, "Quantitative evaluation and intercomparison of morning and afternoon Moderate Resolution Imaging Spectroradiometer (MODIS) aerosol measurements from Terra and Aqua satellites," *J. Geophys. Res.*, vol. 110, no. D10S03, 2005. DOI: 10.1029/2004JD004987.

[44] D. A. Chu, Y. J. Kaufman, L. A. Remer, and B. N. Holben, "Remote sensing of smoke from MODIS airborne simulator during the SCAR-B experiment," *J. Geophys. Res.*, vol. 103, pp. 31 979–31 987, 1998.

[45] M. J. Wooster, B. Zhukov, and D. Oertel, "Fire radiative energy for quantitative study of biomass burning: Derivation from the BIRD experimental satellite and comparison to MODIS fire products," *Remote Sens. Environ.*, vol. 86, pp. 83–107, 2003. 2003.

[46] M. J. Wooster and Y. H. Zhang, "Boreal forest fires burn less intensely in Russia than in North America," *Geophys. Res. Lett.*, vol. 31, no. L20505, 2004. DOI: 10.1029/2004GL020805.

Charles Ichoku (M'0l) received the B.Sc. and M.Sc. degrees in the surveying sciences from the University of Nigeria, Enugu, Nigeria, and the Diplôme d'Etudes Supérieures Specialisées degree in remote sensing and the Ph.D. degree in earth sciences from the Université Pierre et Marie Curie, Paris, France, in 1982, 1987, 1989, and 1993, respectively.

He was a Research Fellow/Visiting Scientist at the Jacob Blaustein Institute for Desert Research, Ben-Gurion University of the Negev, Sede Boker Campus, Israel, from 1993 to 1997, then at the Max-Planck Institute for Chemistry, Mainz, Germany, from 1997 to 1998. His research activities included developing remote sensing applications in various branches of the earth sciences, including geology, hydrology, and atmospheric studies. He joined Science Systems and Applications, Inc., Lanham, MD, working at the NASA Goddard Space Flight Center, Greenbelt, MD, in November 1998, as a Research Scientist. His research interests have been in remote sensing of aerosols and fires, their global distribution, and their impacts on the human population, the environment, and climate. He has been actively involved in the validation and applications of the aerosol and fire products derived from the Moderate-Resolution Imaging Spectroradiometer sensor aboard the EOS Terra and Aqua satellites.

Dr. Ichoku is a member of the American Geophysical Union.

Yoram J. Kaufman received the B.S. and M.S. degrees in physics from the Technion—Israeli Institute of Technology, Haifa, Israel, and the Ph.D. degree from Tel-Aviv University, Tel-Aviv, Israel.

He came to NASA Goddard Space Flight Center (GSFC), Greenbelt, MD, in 1979 on an NRC Fellowship Award. He is currently a Senior Fellow and Atmospheric Scientist at GSFC. He has served as the Project Scientist of the Earth Observing System first satellite EOS-Terra, from 1996 through its launch in December 1999, and was a Member of the MODIS Science Team (1988–2003). His present work includes theoretical and experimental research in atmospheric radiative transfer and remote sensing, including remote sensing of aerosol, their interaction with clouds and radiation, and impact on climate. He conducted the Smoke/Sulfate, Clouds And Radiation (SCAR) field experiments in Brazil and the U.S., to characterize smoke aerosol properties, their emissions from fires, and their effect on clouds and radiation. He has over 170 refereed publications.

Dr. Kaufman is the seventh recipient of the NASA/GSFC Nordberg Award for Earth Sciences and was awarded the NASA Medal for Exceptional Scientific Achievement. He is a Fellow of the American Meteorological Society and is listed among the ISI highly cited scientists in Geophysics.